Morphology and intermolecular dynamics of 1-alkyl-3-methylimidazolium bis{(trifluoromethane)sulfonyl}amide ionic liquids: structural and dynamic evidence of nanoscale segregation

2009 J. Phys.: Condens. Matter 21 424121

(http://iopscience.iop.org/0953-8984/21/42/424121)

J. Phys.: Condens. Matter **21** (2009) 424121 (9pp) doi:10.1088/0953-8984/21/42/424121

Morphology and intermolecular dynamics of 1-alkyl-3-methylimidazolium bis{(trifluoromethane)sulfonyl}amide ionic liquids: structural and dynamic evidence of nanoscale segregation

Olga Russina[1], Alessandro Triolo[1], Lorenzo Gontrani[2], Ruggero Caminiti[2], Dong Xiao[3], Larry G Hines Jr[3], Richard A Bartsch[3], Edward L Quitevis[3], Natalia Plechkova[4] and Kenneth R Seddon[4]

[1] Istituto per i Processi Chimico-Fisici-CNR, Salita Sperone, Contrada Papardo, 98158 Faro Superiore, Messina, Italy
[2] Dipartimento di Chimica, Università di Roma 'Sapienza', Piazzale A Moro, 00185 Roma, Italy
[3] Department of Chemistry and Biochemistry, Texas Tech University, Lubbock, TX 79409-1061, USA
[4] The QUILL Centre, The Queen's University of Belfast, Stranmillis Road, Belfast BT9 5AG, UK

E-mail: triolo@me.cnr.it and edward.quitevis@ttu.edu

Received 22 May 2009, in final form 15 September 2009
Published 29 September 2009
Online at stacks.iop.org/JPhysCM/21/424121

Abstract

Here we report on the structural and dynamical properties of a series of room temperature ionic liquids, namely 1-alkyl-3-methylimidazolium bis{(trifluoromethane)sulfonyl}amide ($[C_n\text{mim}][\text{NTf}_2]$), with varying alkyl chain lengths ($1 \leqslant n \leqslant 10$) at ambient temperature, where all the salts are stable liquids. Using small-wide angle x-ray scattering (SWAXS), three major diffraction peaks are found: two high-Q peaks that show little dependence on the alkyl chain length (n) and a low-Q peak that strongly depends both in amplitude and position on n. This low-Q peak is the signature of the occurrence of nanoscale structural heterogeneities whose sizes depend on the length of the alkyl chain and are related to chain segregation into nano-domains. Using optical heterodyne-detected Raman-induced Kerr effect spectroscopy, we access intermolecular dynamic features that suggest that chain aggregation only occurs for $n \geqslant 3$, in agreement with the SWAXS data. Moreover, the increase in the frequency and width of the main band of the optical Kerr effect spectra in going from $n = 2$ to 3 is consistent with stiffening of the intermolecular potential due to chain segregation. Multicomponent line shape analysis suggests that there are least three modes that underlie the main band in the 0–200 cm^{-1} region of the optical Kerr effect spectra of these ionic liquids. Given the similarity of ionic liquids to other complex fluid systems, we assign the low-frequency component to a fast β-relaxation mode and the intermediate- and high-frequency components to librational modes.

(Some figures in this article are in colour only in the electronic version)

1. Introduction

Room temperature ionic liquids represent an important class of materials from both a fundamental [1] and applied [2] perspective. Ionic liquids are most commonly defined as salts with melting points around about or below 373 K [3]. Usually an ionic liquid is composed of a bulky organic cation and one of a range of common anions, which might be either organic or inorganic, and possesses negligible vapour pressure [4], low flammability and a wide liquid range [3]. The vast number of potential ionic liquids (over a million simple ones and over a trillion ternary systems [5]) means that ionic liquids can be designed specifically with tuneable physicochemical properties, leading to their description as 'designer' solvents [6, 7].

Within a given series of ionic liquids, major changes in physicochemical properties can be induced by simply changing the length of the alkyl side-chains on the cation, especially properties such as melting point, viscosity, density, conductivity and lipophilicity [8, 9]. Here, we report a structural and dynamics investigation of a family of 1-alkyl-3-methylimidazolium salts, characterized by a common anion, bis{(trifluoromethan)sulfonyl}amide ($[C_n\text{mim}][\text{NTf}_2]$), and varying alkyl chain lengths ($1 \leqslant n \leqslant 10$) [10]. This is the first time that such a wide family of salts has been investigated by x-ray scattering and optical heterodyne-detected Raman-induced Kerr effect spectroscopy (OHD-RIKES), thus extracting important structural and dynamical properties. These techniques provide useful information on the microscopic behaviour of these salts, as recent publications have already highlighted [11–15].

Small and wide angle x-ray scattering (SWAXS) is a key tool in accessing morphological details in matter covering a length scale from angstroms to several nanometres. OHD-RIKES is a nonlinear optical time-domain technique that measures the collective polarizability anisotropy dynamics of a liquid [16–19]. By use of a Fourier-transform-deconvolution procedure [20, 21], the OHD-RIKES time-domain data can be converted to a reduced spectral density (RSD) or optical Kerr effect (OKE) spectrum, which is directly related to the depolarized Rayleigh/Raman spectrum of the liquid [22]. Because of its ease of use and the high quality of the resultant data, OHD-RIKES has recently become the most common method for studying the low-frequency intermolecular modes of liquids [18, 19, 23] and, in particular, ionic liquids [13–15, 24–32].

The reported SWAXS data will provide a microscopic picture of the existence of a nanoscale organization in the liquid state of the ionic liquids. Such behaviour has been previously observed in different ionic liquids, but this is the first study of a wide series that includes both even and odd members. Our previous studies [11, 12] on even members of the series of $[C_n\text{mim}][\text{PF}_6]$, $[C_n\text{mim}][\text{BF}_4]$ and $[C_n\text{mim}][\text{Cl}]$ showed that a low-Q (momentum transfer) peak can be observed in the diffraction pattern from salts bearing a long enough alkyl chain, in agreement with structural findings from molecular dynamics (MD) simulations [33–35]. MD simulations indicate that, as a consequence of the amphiphilic nature of the cation, the polar heads and the alkyl chains tend to segregate, thus leading to structural domains whose average size depends on the alkyl chain length [34, 35]. Experimental evidence for the existence of such an organization was previously found in diffusion [36], Raman spectroscopic (linear and nonlinear) [37, 38] and OKE spectroscopic measurements [13–15]. The x-ray diffraction data from our group (for imidazolium salts), from Mizuhata *et al* (for aliphatic quaternary ammonium salts) [39] and the neutron diffraction data from Atkin and Warr [40] (for alkylammonium salts) confirm this scenario, providing a clear quantitative description of the nature of this phenomenon.

2. Experimental details

2.1. Synthesis

The synthesis of the $[C_n\text{mim}][\text{NTf}_2]$ compounds has been described previously [41].

2.2. Energy dispersive x-ray diffraction

Energy dispersive x-ray diffraction (EDXD) experiments were done using the non-commercial energy-scanning diffractometer built at the Department of Chemistry, University of Rome. Detailed descriptions of both the instrument and technique can be found in several papers [42–45]. Transmission geometry was employed. The momentum transfer range between 0.12 and 19.56 Å^{-1} was accessed. The measuring time was 300 000 counts per experimental point for $q < 5$ Å^{-1} and 600 000 counts for $q > 5$ Å^{-1}. Corrections for absorption and incoherent scattering were applied, using our program DIF1.

2.3. SWAXS

The SWAXS experiments were conducted at the high brilliance beam line ID02 at the European Synchrotron Radiation Facility (ESRF), Grenoble, France [46], using an instrumental setup which allows coverage of the momentum range Q between 0.1 and 2 Å^{-1}, with a wavelength $\lambda = 0.75$ Å (energy = 16.5 keV). Measurements were collected at 25 °C, using a thermostatted bath, and the sample was kept inside a temperature-controlled, flow-through cell with an internal diameter of 1.9 mm. The corresponding empty cell contribution was subtracted. Calibration to absolute units (mm^{-1}) was obtained using a neat water sample in a 2 mm capillary.

2.4. OHD-RIKES

The titanium-sapphire (TiS) laser, optical delay line and pump–probe configuration were the same as previously reported [15]. The current version of the OHD-RIKES apparatus uses a Coherent Verdi V6 diode-pumped solid-state laser to pump the TiS laser. With this pump laser, the TiS laser generates 36 fs pulses as determined from the background-free pulse-intensity autocorrelation. The apparatus uses balanced detection and compensates for drift and fluctuations in the laser intensity to increase the signal-to-noise ratio [18]. To save data collection time, scans were carried out in 10 fs steps for time delays

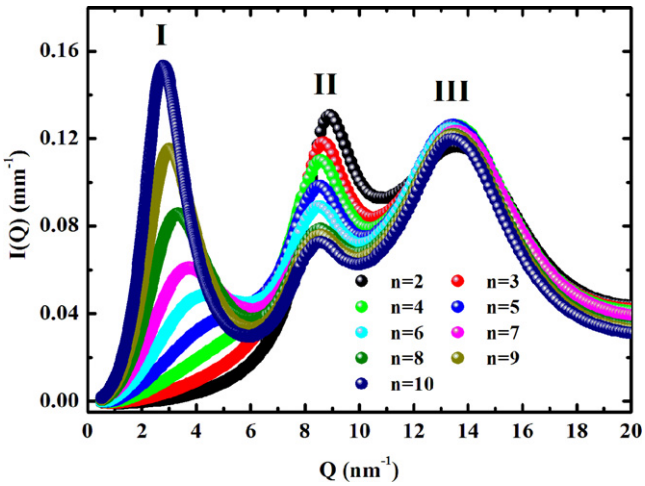

Figure 1. SWAXS data for the series $[C_n\text{mim}][\text{NTf}_2]$ with $n = 2$–10. Data were collected at the ID02 beamline at room temperature.

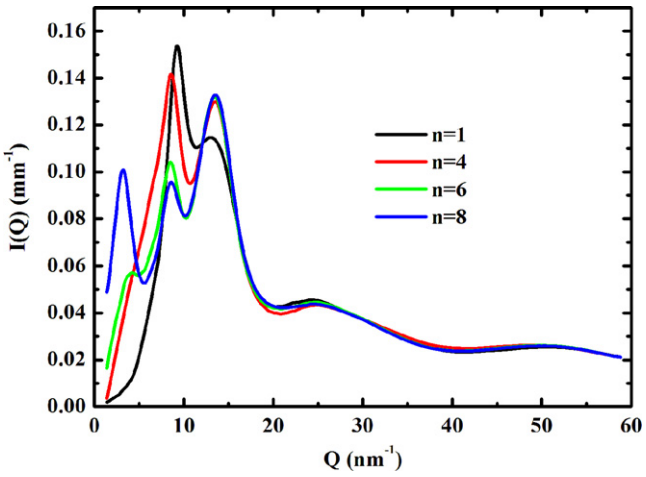

Figure 2. SWAXS data for the series $[C_n\text{mim}][\text{NTf}_2]$ with $n = 1$, 4, 6, or 8. Data were collected at room temperature using an EDXD diffractometer.

between −1 and 4 ps and in 100 fs steps for time delays between 4 and 10 ps. Each OHD-RIKES signal is an average of at least eight scans. All data were obtained at a heterodyne angle of 2°. Samples for the OHD-RIKES measurements were prepared in a glove box by transferring an aliquot of an ionic liquid to a 2 mm path-length, UV-grade, fused-silica cell (Hellma Cells) with a vacuum stopcock valve. The sample cell was then placed on a vacuum line and heated overnight at 80 °C under vacuum to further reduce the water content. The water content of samples prepared in this way was $\leqslant 100\ \mu\text{g g}^{-1}$, as determined by Karl-Fisher titration. During an OHD-RIKES measurement, a lab-built copper cell holder whose temperature was regulated and controlled with a thermoelectric heater/cooler system kept the sample temperature constant at 295 K. The OHD-RIKES responses in the time range 0.5 ps $< t <$ 10 ps were fitted by the empirical decay function. The fit parameters were used to remove the part of the response that decays on a picosecond or longer timescale to yield a reduced response. The Fourier-transform-deconvolution procedure was then applied to the reduced response to obtain the RSD [20, 21]. Application of a Gaussian window function prior to this procedure helped to smooth the data [47].

3. Results and discussion

3.1. Small-wide angle x-ray scattering (SWAXS) data

In figure 1 we report the SWAXS patterns collected at ID02 from the whole series of samples $[C_n\text{mim}][\text{NTf}_2]$ with $n = 2$–10. Moreover, in figure 2, data collected with the EDXD setup are shown for a selection of samples including $[C_1\text{mim}][\text{NTf}_2]$ (namely $[C_n\text{mim}][\text{NTf}_2]$ with $n = 1, 4, 6, 8$). Three major diffraction features can be noticed in both data sets: (a) a peak (hereafter indicated as peak III) at high Qs that is rather unaffected (both in amplitude and peak position (approx. 14 nm^{-1})) by the alkyl chain length (although the ID02 data for $[C_2\text{mim}][\text{NTf}_2]$ and the EDXD data for $[C_1\text{mim}][\text{NTf}_2]$ show a decrease in its amplitude as compared to the other members of the series); (b) a peak at intermediate Qs (hereafter indicated as peak II) that is centred at high Q values for $n = 1$ and 2 ($Q = 9.2$ and 8.9 nm^{-1}, respectively) and then becomes constant at approximately 8.5 nm^{-1} for higher n values, and whose amplitude increases with decreasing n; and (c) a peak at low Qs that is strongly affected by n both in its amplitude and position (hereafter indicated as peak I). The EDXD data were collected over a wider Q range than the one accessible at ID02. For Q values higher than approximately 20 nm^{-1} the x-ray diffraction patterns from the EDXD data do not show major differences between members of the series $[C_n\text{mim}][\text{NTf}_2]$ with varying n. This is in part due to the fact that a consistent part of the scattering arises from the $[\text{NTf}_2]^-$ anion and might also imply that at short spatial range ($r <$ 2–3 Å) the different salts have the same morphology. We showed some of the ID02 data (namely for the series $[C_n\text{mim}][\text{NTf}_2]$ with $n = 2$–5) in a previous publication [32] and are reporting the data for the longer alkyl chains and the EDXD data in this paper for the first time.

While peaks II and III are essentially related to first neighbour interactions or to intramolecular structural correlations and as such are quite common for molecular liquids (here we stress that peak II is characteristic of $[\text{NTf}_2]^-$-containing ionic liquids), peak I is a feature that has been observed in only a few classes of materials, such as alcohols. This peak is a consequence of the existence of structural heterogeneities with nanometre spatial scale and is rather ubiquitous in ionic liquids, reflecting the amphiphilic nature of these materials. Previous indications of the existence of such diffraction features have been provided for other ionic liquids, including $[C_n\text{mim}][\text{Cl}]$, $[C_n\text{mim}][\text{BF}_4]$, $[C_n\text{mim}][\text{PF}_6]$ [11, 12], AAN (alkylammonium nitrates, with alkyl=ethyl and propyl) [40], AQAs (aliphatic quaternary salts) [39] and, as mentioned, $[C_n\text{mim}][\text{NTf}_2]$ [32].

In order to estimate the characteristic sizes of the structural heterogeneities that characterize the neat room temperature ionic liquid morphology from peak I positions, we use Bragg's law ($D = 2\pi/Q_{\text{MAX}}$) as an approximation. Such sizes show a linear dependence on the alkyl chain length, n. The

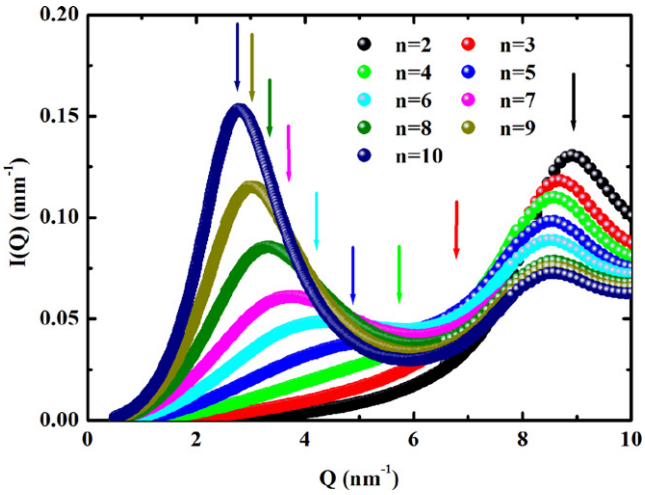

Figure 3. Low-Q portion of the SWAXS data for the series $[C_n\text{mim}][\text{NTf}_2]$ with $n = 2$–10. Data were collected at the ID02 beamline at room temperature. The arrows indicate the position of the peak at low Q, as obtained either from the fit with a Gaussian function ($n \geqslant 6$) or from the extrapolation of the linear behaviour proposed in figure 4 ($2 \leqslant n \leqslant 5$).

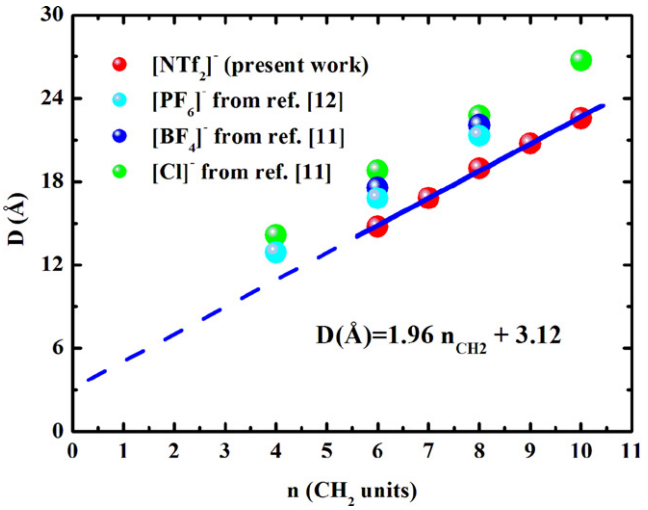

Figure 4. Alkyl chain length dependence of the characteristic size of the nanoscale heterogeneities as obtained from the low-Q peak position from the SWAXS data for the $[C_n\text{mim}][\text{NTf}_2]$ series. The other symbols refer to the same quantity obtained from SWAXS data from the $[C_n\text{mim}][\text{Cl}]$, $[C_n\text{mim}][\text{BF}_4]$, $[C_n\text{mim}][\text{PF}_6]$ series. The continuous blue line refers to the linear fit of the data for $n \geqslant 6$. The dashed blue line represents the extrapolation of such a linear trend to lower n values.

present data sets explore in a systematic way a much wider range corresponding to $n = 2$–10 for the case of the asymmetric $[C_n\text{mim}]^+$ salts and provide a unique basis for testing structural models to account for the nano-segregation effects in ionic liquids.

In figure 3, a selected region of the spectrum of figure 1 is plotted, highlighting the low-Q portion. By fitting peak I by a Gaussian function, one can estimate its position, Q_{MAX}, and derive the characteristic size. This procedure was applied to the longer alkyl chain salts ($6 \leqslant n \leqslant 10$). However, for shorter alkyl chain salts, we could not reliably estimate Q_{MAX} for peak I due to the peak merging with the tail of peak II. In figure 4 the alkyl chain dependence of the characteristic size, D, is plotted. Together with the data from the present series, we also show in this figure the corresponding findings from imidazolium salts with PF_6^-, BF_4^- and Cl^- anions from our previous studies [11, 12].

Several features can be noticed from this graph. The data for the $[\text{NTf}_2]^-$ series exhibit a linear trend which is fitted by the equation $D_{\text{fit}}(\text{Å}) = 1.96n + 3.12$. The slope of this trend ($\partial D_{\text{NTf2}}/\partial n = 1.96$ Å/CH_2 units) is similar to the one found for the other imidazolium-based salts ($\partial D_{\text{PF6}}/\partial n = \partial D_{\text{Cl}}/\partial n = 2.1$ Å/CH_2 units) investigated previously [11, 12]. From the linear trend highlighted (and extrapolated to lower n values) in figure 4, one can estimate the position of peak I that would be observed in the SAXS data if it were not (partially) obscured by peak II at higher Qs. In figure 3, the vertical arrows indicate the Q values where the extrapolated peaks should occur on the basis of the linear trend indicated in figure 4. One observes that, apart from the positions of the first five peaks ($6 \leqslant n \leqslant 10$) that were explicitly modelled with a Gaussian function to estimate peak positions, the other peaks are not easily discernible as they are hidden by the tail of peak II. Nevertheless, the extrapolation from the linear trend proposed in figure 4 seems to properly estimate the peak positions, at least for the case $n > 3$.

It is noteworthy that the distinct shift to higher Q values of peak II in the case of $n = 2$, with respect to the position of the same peak for $n \geqslant 3$, might be a consequence of the occurrence of peak I at approximately 8.5 nm^{-1}. This would imply that peaks I and II are strongly superimposed. However, the extrapolated value for the case of $n = 1$ would be about $Q = 12.2$ nm^{-1}, which falls in a range where no features related to a peak are observed in the corresponding diffraction pattern. We propose that the shift of the peak II position that is observed for the cases of $n = 1$ and 2 as compared to higher members of the series is due to a different effect than the occurrence of a 'nanoscale segregation' effect. If one considers that $[C_n\text{mim}][\text{Cl}]$ salts do not show the peak II that is found in the present series of salts, one is led to relate such a peak to the spatial correlation of the $[\text{NTf}_2]^-$ anion with either the cations or other anions.

Accordingly, the present data seem to indicate that (a) only for $n \geqslant 3$ are there indications of an excess scattering intensity (i.e. a '*nanoscale segregation*'-related peak, that might be hidden in the case of short alkyl chains) for $Q < 7$ nm^{-1} with respect to the diffraction patterns from salts with $n = 1$ or 2 and (b) in the case of $[C_n\text{mim}][\text{NTf}_2]$ with $n = 1$ and 2, the anion interaction with either neighbouring anions or cations is characterized by a shorter interaction distance than found for the case of $n \geqslant 3$, presumably as a consequence of the reduced steric hindrance due to the methyl/ethyl side groups on the cations.

We also notice that although the observed trends for D versus n for the various anions are essentially parallel (figure 4), the intercept of the trend line distinctly depends on

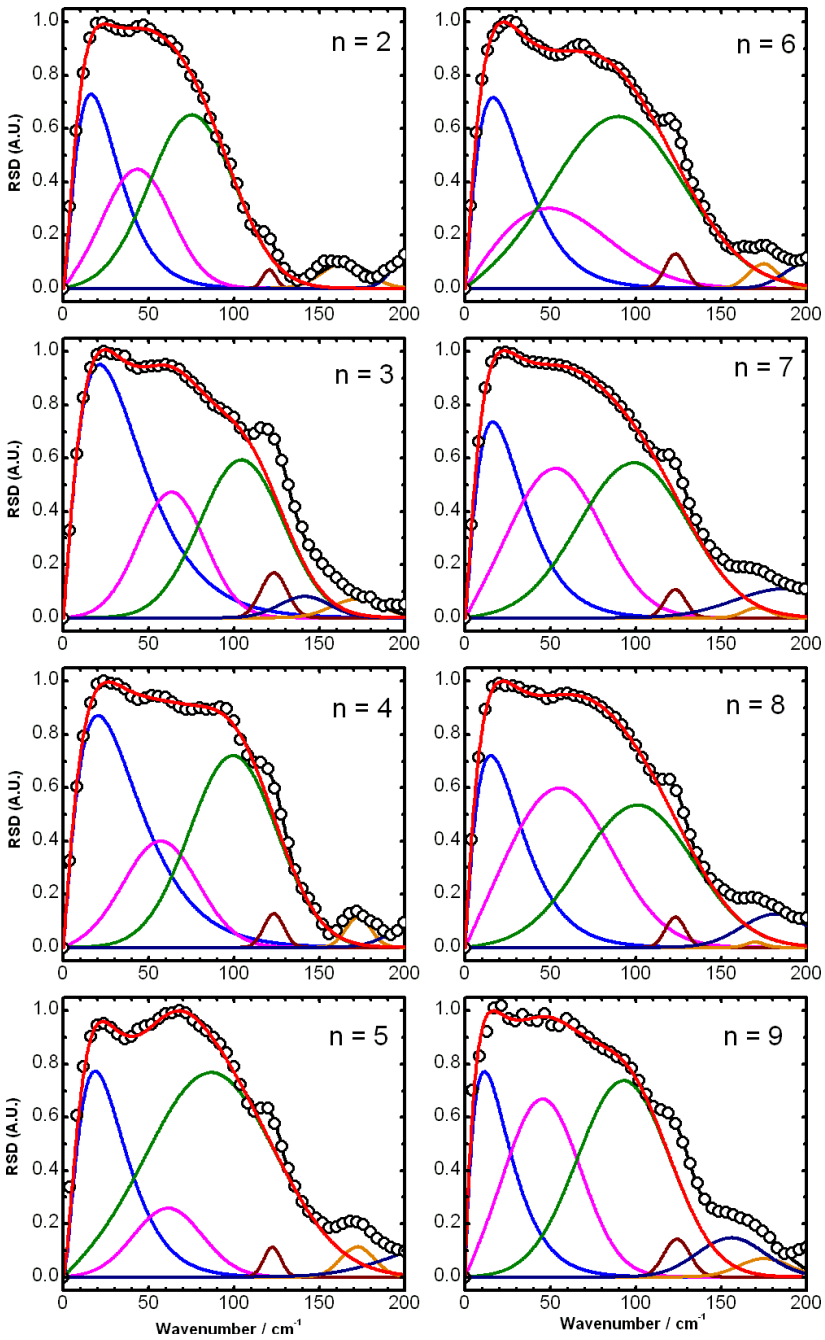

Figure 5. Reduced spectral densities for $[C_n\text{mim}][\text{NTf}_2]$ with $n = 2$–9 at 295 K. The solid lines through the data points are fits of the multicomponent line shape model to the reduced spectral densities. Component bands obtained in the multicomponent analysis of the reduced spectral densities are also shown. Solid red curves are fits of three-component model to the main band. See table 1 for the spectral parameters.

the nature of the anion. In particular, the larger the anion, the smaller the intercept.

3.2. Reduced spectral densities (RSDs)

Giraud *et al* [25] showed that the RSDs of imidazolium ionic liquids consist of a broad band between 0 and 200 cm^{-1} and a low-intensity high-frequency tail that extends out to several hundred wavenumbers. Because of the limitations of our OHD-RIKES apparatus, we were unable to obtain reproducible data beyond 250 cm^{-1}. Therefore, we will mainly focus on the RSDs in the 0–200 cm^{-1} region. The OKE spectra of $[C_n\text{mim}][\text{NTf}_2]$ with $n = 2, 4, 5, 6$ and 8 were first reported by us in a preliminary study [24]. As a result of improvements in the OHD-RIKES apparatus, we are now able to obtain OKE spectra that are of higher quality than those reported in the preliminary study. The OKE spectra at 295 K for $[C_n\text{mim}][\text{NTf}_2]$, as well for the symmetric $[(C_n)_2\text{im}][\text{NTf}_2]$ ionic liquids, with $n = 2$–5 were recently reported [32]. This current paper extends the previous study to longer alkyl chains with $n = 6$–9.

The RSDs shown in figure 5 are characterized by narrow intramolecular bands and a broad intermolecular band. The intramolecular band at $\approx$120 cm^{-1}, which is a distinct feature

Table 1. Spectral parameters for intermolecular part of OKE spectra of ionic liquids [$C_n$mim][NTf_2] in the 0–200 cm^{-1} region at 295 K. (Note: $\langle\omega\rangle$—first spectral moment $\langle\omega\rangle \equiv \int \omega I(\omega)\,d\omega / \int I(\omega)\,d\omega$ where $I(\omega)$ is the spectral density or component band with integration limits 0–200 cm^{-1}; $\Delta\omega$, full-width-at-half-maximum; area, relative fractional area; error in $\langle\omega\rangle$ and $\Delta\omega = \pm 2$ cm^{-1}.)

	Main band[a]		Component 1			Component 2			Component 3		
n	$\langle\omega\rangle$ cm^{-1}	$\Delta\omega$ cm^{-1}	$\langle\omega\rangle$ cm^{-1}	$\Delta\omega$ cm^{-1}	Area	$\langle\omega\rangle$ cm^{-1}	$\Delta\omega$ cm^{-1}	Area	$\langle\omega\rangle$ cm^{-1}	$\Delta\omega$ cm^{-1}	Area
2	53.9	88.9	26.4	30.9	0.28	44.8	46.9	0.25	75.5	58.8	0.47
3	66.1	114.9	38.8	46.9	0.45	63.6	45.9	0.21	104.4	57.8	0.34
4	67.1	116.8	37.4	45.3	0.39	57.7	51.7	0.19	99.6	60.4	0.42
5	70.4	114.6	29.5	34.2	0.26	61.6	47.7	0.12	88.6	88.7	0.62
6	69.1	116.0	29.2	35.1	0.25	58.7	74.9	0.21	91.2	90.5	0.54
7	67.4	114.3	28.4	34.1	0.25	55.8	62.8	0.33	99.1	76.3	0.42
8	68.2	117.1	27.9	33.8	0.24	59.7	71.0	0.38	101.1	77.8	0.38
9	62.8	113.8	22.6	27.6	0.22	47.4	51.9	0.33	92.9	63.8	0.45

[a] The main band is a superposition of component bands 1–3.

in the RSDs of these ionic liquids, is commonly assigned to an intramolecular vibration of the $[NTf_2]^-$ ion [25]. A second less intense band peak at ≈170 cm^{-1}, also commonly assigned to an intramolecular vibration of the $[NTf_2]^-$, can be seen in some of the RSDs [25]. The presence of the 170 cm^{-1} peak in the RSDs is partly determined by the signal-to-noise ratio of the time-domain response. It is clearly present in the OKE spectra of some ionic liquids but absent in the OKE spectra of other ionic liquids. A possible reason for this is that the amplitude of the oscillatory component in the OHD-RIKES signal associated with this intramolecular vibration tends to be comparable to that of the noise. Consequently, it can be removed by the Gaussian window function, which is applied to the OHD-RIKES signal to reduce the noise.

Xiao *et al* [13, 14] have suggested that the RSD of an ionic liquid largely reflects the intermolecular dynamics in the polar regions of the ionic liquid. To see this we must first understand the molecular motions underlying the RSD of an ionic liquid. In general, the RSD of a liquid will have contributions from a molecular term, an interaction-induced term, and a molecular-interaction-induced cross term [48]. The RSD for most liquids, however, tends to be dominated by the molecular term, which arises from the collective motion of the molecules in the liquid [48]. For ionic liquids consisting of an organic cation and an inorganic anion, the RSD is largely determined by the motion of the cation. This clearly is the case for ionic liquids with spherical anions. To show this for ionic liquids with nonspherical inorganic anions, we make use of the dependence of the RSD on the square of the derivative of the polarizability anisotropy, $(\partial\Pi_{anis}/\partial q)^2$, where q is a canonical coordinate associated with one of the modes of the liquid, to estimate the relative contributions of the various motions of the liquid to the RSD [48]. Giraud *et al* [25] showed that the value of $(\partial\Pi_{anis}/\partial q)^2$ for the imidazolium ring is a factor of $\sim 4 \times 10^{13}$ times greater than that of the $[NTf_2]^-$ ion. Recent MD simulations on 1-methoxyethylpyridinium dicyanoamide (MOEPy^+/DCA$^-$) confirm that the OHD-RIKES response is indeed dominated by the reorientational dynamics of the cation [49].

The intermolecular part of the RSD of [C_2mim][NTf_2] is characterized by a main band with a width of ≈100 cm^{-1}. In contrast, the RSDs for n = 3–9 are dominated by a main band that is considerably broader and higher in frequency than the corresponding band in the RSD of [C_2mim][NTf_2]. To provide a more quantitative description of these patterns, the RSDs were subjected to multicomponent line shape analysis. In this analysis, the lowest-frequency component is represented by the Bucaro–Litovitz (BL) line shape function, and the higher-frequency components and the intramolecular bands by the antisymmetrized Gaussian (AG) line shape function. As can be seen in figure 5, the intermolecular part of the RSDs in the 0–200 cm^{-1} region is well fitted by a BL function and three AG functions.

The main band in the 0–200 cm^{-1} region can best be described by a three-component model, comprising a low-frequency component, an intermediate-frequency component and a high-frequency component (bands 1, 2 and 3). Rajian *et al* [26] previously found that two bands adequately described the main band of the intermolecular part of the RSD of [C_5mim][NTf_2]. The use of a three-component model provides a more accurate description of the line shape of this band. Indeed, Rajian *et al* showed that the temperature dependence of the high-frequency component in the two-component model can be resolved into a temperature-independent part and temperature-dependent part. The solid red curves in figure 5 are fits of the three-component model to the low-frequency band. Values of first spectral moment $\langle\omega\rangle$ and the full-width-at-half-maximum, $\Delta\omega$, for the main band in the intermolecular part of the RSD and the underlying component bands are listed in table 1.

For comparison, fits of the three-component model to the main band are plotted together in figure 6. This figure shows that the width of the main band with n = 3–9 is relatively independent of the length of the alkyl chain. This pattern is clearly evident when $\langle\omega\rangle$ and $\Delta\omega$ are plotted against the number of carbon atoms in the alkyl chain (figure 7(a)): $\langle\omega\rangle$ increases from 54 ± 1 cm^{-1} at n = 2 to an average value of 68 ± 2 cm^{-1} for n = 3–9 and $\Delta\omega$ increases from 89 cm^{-1} at n = 2 to an average value of 115 ± 1 cm^{-1} for n = 3–9. Based on the three-component model, the increase in frequency and width of the main band in going from n = 2 to 3 is largely due to the shift to higher frequency and broadening of the high-frequency component.

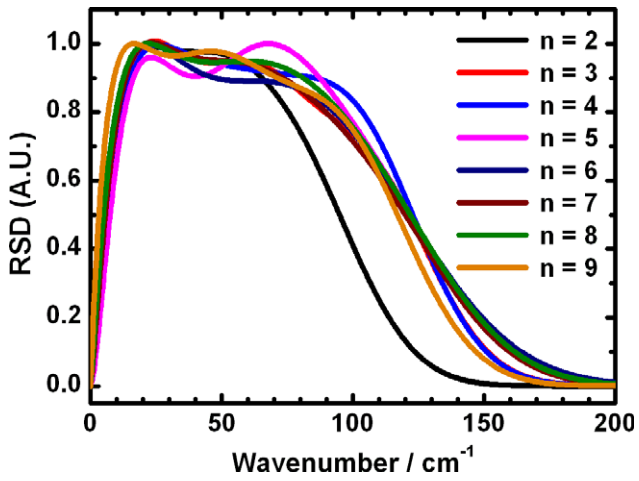

Figure 6. Comparison of fits of the three-component model (see text) to the main band in OKE spectra of $[C_n\text{mim}][\text{NTf}_2]$ with $n = 2$–9.

If the $[C_n\text{mim}][\text{NTf}_2]$ for $n \geqslant 3$ are nano-segregated as x-ray diffraction measurements indicate, then the increase in frequency and width of the main band in going from $n = 2$ to 3 makes physical sense. This can be seen as follows. Clearly, the Coulombic interaction between the imidazolium ring, where most of the positive charge resides, and the anion will be a common term in the intermolecular potential for all the $[C_n\text{mim}][\text{NTf}_2]$ ionic liquids. However, because the imidazolium ring is tethered to the alkyl chain, additional terms in the intermolecular potential will arise for $n \geqslant 3$ due to tail segregation that results in the formation of nonpolar domains. Consequently, the imidazolium rings will see a stiffer intermolecular potential, which is manifested by higher-frequency contributions to the OKE spectrum. Moreover, that the frequency and width of the main band are basically independent of alkyl chain length is further evidence that the intermolecular part of OKE spectra for $n \geqslant 3$ reflects the dynamics in the polar regions of the ionic liquid.

In addition to the variation of $\langle\omega\rangle$ and $\Delta\omega$ with respect to n, there are subtle variations in the shape of the main band that are more difficult to quantify. The principal variation is associated with the shape of the main band as reflected in the relative intensities of the low- and high-frequency shoulders of the band. This particular dependence of the line shape on the cation appears to be well described by the parameter $\rho_{(\text{I+H})/\text{L}}$, which is defined as the ratio of the sum of the areas of the intermediate- and high-frequency component bands to the area of the low-frequency component. As can be seen in figure 7(b), $\rho_{(\text{I+H})/\text{L}}$ exhibits three regimes: $n = 2$–3 (regime 1); $n = 3$–5 (regime 2) and $n = 5$–9 (regime 3). In regime 1, $\rho_{(\text{I+H})/\text{L}}$ decreases from 2.5 to 1.2 in going from $n = 2$ to 3. This change is not surprising given that $\langle\omega\rangle$ and $\Delta\omega$ also change. Moreover, the change in all three spectral parameters provides further support for the possibility that already in the case of a propyl side chain, alkyl chain segregation is occurring, as indicated by the SWAXS data. However, in contrast to $\langle\omega\rangle$ and $\Delta\omega$, which appear to be independent of alkyl chain length for $n = 3$–9, $\rho_{(\text{I+H})/\text{L}}$ exhibits a dependence on alkyl chain length that is characterized by a sharp increase in going from

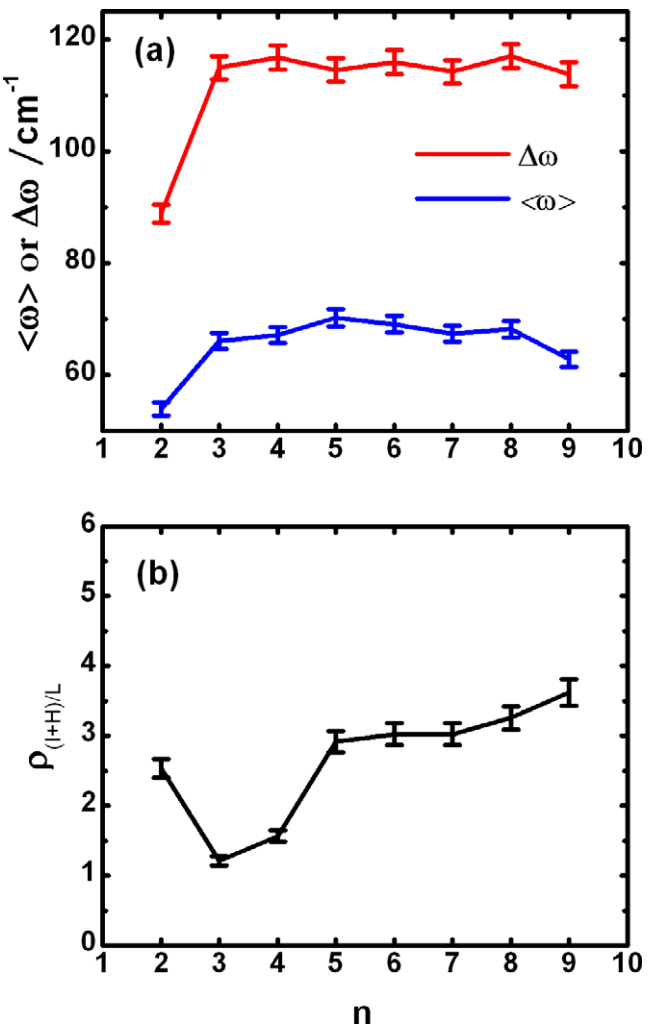

Figure 7. (a) Plot of the first spectral moment, $\langle\omega\rangle$, and full-width-at-half-maximum $\Delta\omega$ of the main band versus n. (b) Plot of the ratio $\rho_{(I+H)/L}$ corresponding to the sum of the areas of the intermediate- and high-frequency components (bands 2 and 3) relative to the area of the low-frequency component (band 1).

$n = 3$ to 5 with a slope $\partial\rho_{(\text{I+H})/\text{L}}/\partial n = 0.7 \pm 0.4$ followed by a gradual increase in going from $n = 5$ to 9 with a slope $\partial\rho_{(\text{I+H})/\text{L}}/\partial n = 0.16 \pm 0.04$.

Although multicomponent line shape analysis is commonly used to provide a quantitative description of RSD, there is no *a priori* reason to assume the component bands correspond to actual modes of a simple liquid. Even for nonassociating liquids composed of simple symmetric top molecules, a molecular approach combining MD simulations and detailed theoretical analysis is needed to extract information about the microscopic origins of an OKE spectrum [48, 50–52]. However, for complex systems, such as associating liquids [53] and supercooled liquids [54, 55], the lowest-frequency modes, which are collectively referred to as structural relaxation, are typically characterized by librational modes at high frequencies (greater that 1 THz or 33 cm^{-1}), and by α-relaxation modes at low frequencies. At frequencies higher than that of the α-relaxation, additional modes are observed known as intermediate, secondary or β relaxations, which are varied but

often not well understood. In supercooled liquids, the slowest of the β-relaxations is the Johari–Goldstein relaxation mode, which is associated with transient cages [56]. The α- and β-relaxations are distinguished by temperature dependences that diverge from each other as the glass transition is approached from above.

As recent OKE experiments [57, 58] over a broad range of times and temperatures down to the glass transition have shown, ionic liquids appear to be similar to that of other complex systems in that the low-frequency modes are also characterized by α- and β-relaxations. In the 0–10 ps time window of our measurements, the molecular motions probed in our OHD-RIKES measurements on $[C_n\text{mim}][\text{NTf}_2]$ are mainly associated with the slow and fast β-relaxations and librational dynamics. By removing contributions to the OHD-RIKES response with relaxation times greater than 1 ps, only the fast β-relaxations and librational modes are retained in the reduced response.

In the frequency-domain representation of the reduced response, the lowest-frequency component (band 1) corresponds to the fast β-relaxation, and the intermediate- and high-frequency components (bands 2 and 3) to librational modes. For $n = 3$–9, the assignment of component 1 to an actual mode of the liquid is further supported by the fact that its frequency, as measured by first spectral moment $\langle\omega\rangle$, and width $\Delta\omega$ vary systematically with alkyl chain length, with $\langle\omega\rangle$ decreasing from 38.8 to 22.6 cm^{-1} and $\Delta\omega$ increasing from 46.9 to 27.6 cm^{-1} as n increases from 3 to 9. Moreover, based on this interpretation of the component bands, the parameter $\rho_{(\text{I+H})/\text{L}}$ measures the relative contributions of the librational and relaxation modes to the main band of the OKE spectra of these ionic liquids. In particular, the plot in figure 7(b) tells us how changes in the alkyl chain length affect the relative contributions of relaxation and librational modes to the OKE spectrum of an ionic liquid. For $[C_n\text{mim}][\text{NTf}_2]$ with long alkyl chains ($n = 5$–9), the relative contributions of the relaxation and librational modes to the OKE spectrum depend weakly on chain length, whereas for $[C_n\text{mim}][\text{NTf}_2]$ with short chains ($n = 2$–3), the relative contributions of the relaxation and librational modes to the OKE spectrum exhibit a strong dependence on chain length. Unfortunately, a molecular explanation for this difference in the behaviour of $\rho_{(\text{I+H})/\text{L}}$ for $n = 3$ and 4 as compared to that for $n = 5$–9 is not known at this time.

4. Concluding remarks

This is the first study of the structure and intermolecular dynamics of a complete series of ionic liquids based on the $[C_n\text{mim}]^+$ cation for n both even and odd. The appearance of a peak at low Q in the SWAXS data whose position Q_{max} shifts to lower Q values as n increases is consistent with the existence of heterogeneities. Moreover, the linear dependence of the spatial extent of the heterogeneities, as obtained by the Bragg's law relation, $D = 2\pi/Q_{\text{MAX}}$, with n ($6 \leqslant n \leqslant 10$) is consistent with molecular dynamics simulations that indicate nano-segregation of the alkyl tails. Further analysis of the SWAXS for $n < 6$ suggests the onset of nano-aggregation at $n = 3$. Multicomponent analysis of the main band in the 0–200 cm^{-1} region of the OKE spectra of these ionic liquids clearly indicates a difference in the intermolecular dynamics for $n = 2$ as compared to $n = 3$–9, with $\langle\omega\rangle$ increased from 54 ± 1 cm^{-1} at $n = 2$ to an average value of 68 ± 2 cm^{-1} for $n = 3$–9 and $\Delta\omega$ increasing from 89 cm^{-1} at $n = 2$ to an average value of 115 ± 1 cm^{-1} for $n = 3$–9. This behaviour parallels the onset of nano-aggregation for $n \geqslant 3$ evidenced by the SWAXS data. Indeed the increase in $\langle\omega\rangle$ and $\Delta\omega$ in going from $n = 2$ to 3 (and the corresponding stiffening of the intermolecular potential) can be rationalized by considering that the heterogeneity is a consequence of tail segregation. Moreover, that the frequency and width of the lowest frequency of a three-component model of the main band vary systematically with chain length suggests that the component bands have physical significance. Given the similarity of ionic liquids to other complex fluid systems, we assign the low-frequency component to a fast β-relaxation mode and the intermediate- and high-frequency components to librational modes. The molecular origin of the fast β-relaxation mode and the explanation for the variation of the $\rho_{(\text{I+H})/\text{L}}$ with n are, however, unresolved and will be the subject of future research in our laboratories.

Acknowledgments

This research was supported by the National Science Foundation under grant CHE-0718678 to ELQ. Acknowledgement for partial support of this research is also made to the Donors of the American Chemical Society Petroleum Research Fund under grant 47615-AC6 to ELQ and to The Welch Foundation to RAB under grant D-0775. OR and AT acknowledge the European Synchrotron Radiation Facility for provision of synchrotron radiation facilities and thank Dr E Di Cola and T Narayanan for their kind and competent assistance in exploiting beamline ID02. AT also acknowledges the hospitality of the Helmholtz Zentrum Berlin during the period of this study. NVP and KRS are grateful to the Industrial Advisory Board of QUILL and the EPSRC (Portfolio Partnership Scheme, grant number EP/D029538/1) for their continuing support.

References

[1] Wasserscheid P and Welton T (ed) 2007 *Ionic Liquids in Synthesis* (Weinheim: Wiley–VCH)
[2] Plechkova N V and Seddon K R 2008 *Chem. Soc. Rev.* **37** 123
[3] Stark A and Seddon K R 2007 *Kirk-Othmer Encyclopedia of Chemical Technology* ed A Seidel (Hoboken, NJ: Wiley) p 836
[4] Earle M J, Esperanca J M S S, Gilea M A, Lopes J N A C, Rebelo L P N, Magee J W, Seddon K R and Widegren J A 2006 *Nature* **439** 831
[5] Seddon K R 1999 *The Int. George Papatheodorou Symp.: Proc.* ed S Boghosian, V Dracopoulos, C G Kontoyannis and G A Voyiatzis (Patras: Institute of Chemical Engineering and High Temperature Chemical Processes) p 131
[6] Freemantle M 1998 *Chem. Eng. News* **76** 32
[7] Plechkova N V and Seddon K R 2007 *Methods and Reagents for Green Chemistry: An Introduction* ed P Tundo, A Perosa and F Zecchini (New York: Wiley) p 105
[8] Gordon C M, Holbrey J D, Kennedy A R and Seddon K R 1998 *J. Mater. Chem.* **8** 2627

[9] Holbrey J D and Seddon K R 1999 *Clean Prod. Process.* **1** 223
[10] Holbrey J D, Reichert W M and Rogers R D 2004 *J. Chem. Soc. Dalton Trans.* **15** 2267
[11] Triolo A, Russina O, Bleif H-J and Di Cola E 2007 *J. Phys. Chem.* B **111** 4641
[12] Triolo A, Russina O, Fazio B, Triolo R and Di Cola E 2008 *Chem. Phys. Lett.* **457** 362
[13] Xiao D, Rajian J R, Li S, Bartsch R A and Quitevis E L 2006 *J. Phys. Chem.* B **110** 16174
[14] Xiao D, Rajian J R, Cady A, Li S, Bartsch R A and Quitevis E L 2007 *J. Phys. Chem.* B **111** 4669
[15] Xiao D, Rajian J R, Hines L G Jr, Li S, Bartsch R A and Quitevis E L 2008 *J. Phys. Chem.* B **112** 13316
[16] McMorrow D, Lotshaw W T and Kenney-Wallace G A 1988 *IEEE J. Quantum Electron.* **24** 443
[17] Castner E W Jr and Maroncelli M 1998 *J. Mol. Liq.* **77** 1
[18] Fourkas J T 2001 *Ultrafast Infrared and Raman Spectroscopy* ed M D Fayer (New York: Dekker) p 473
[19] Smith N and Meech S R 2002 *Int. Rev. Phys. Chem.* **21** 75
[20] McMorrow D 1991 *Opt. Commun.* **86** 236
[21] McMorrow D and Lotshaw W T 1991 *J. Phys. Chem.* **95** 10395
[22] Kinoshita S, Kai Y, Yamaguchi M and Yagi T 1995 *Phys. Rev. Lett.* **75** 148
[23] Hunt N T, Jaye A A and Meech S R 2007 *Phys. Chem. Chem. Phys.* **9** 2167
[24] Hyun B R, Dzyuba S V, Bartsch R A and Quitevis E L 2002 *J. Phys. Chem.* A **106** 7579
[25] Giraud G, Gordon C M, Dunkin I R and Wynne K 2003 *J. Chem. Phys.* **119** 464
[26] Rajian J R, Li S, Bartsch R A and Quitevis E L 2004 *Chem. Phys. Lett.* **393** 372
[27] Shirota H, Funston A M, Wishart J F and Castner E W Jr 2005 *J. Chem. Phys.* **122** 184512(1)
[28] Shirota H and Castner E W Jr 2005 *J. Phys. Chem.* A **109** 9388
[29] Shirota H and Castner E W Jr 2005 *J. Phys. Chem.* B **109** 21576
[30] Shirota H, Wishart J F and Castner E W Jr 2007 *J. Phys. Chem.* B **111** 4819
[31] Castner E W Jr, Wishart J F and Shirota H 2007 *Acc. Chem. Res.* **40** 1217
[32] Xiao D, Hines L G Jr, Li S, Bartsch R A, Quitevis E L, Russina O and Triolo A 2009 *J. Phys. Chem.* B **113** 6426
[33] Urahata S M and Ribeiro M C C 2003 *Phys. Chem. Chem. Phys.* **5** 2619
[34] Wang Y and Voth G A 2005 *J. Am. Chem. Soc.* **127** 12192
[35] Lopes J N A C and Padua A A H 2006 *J. Phys. Chem.* B **110** 3330
[36] Tokuda H, Hayamizu K, Ishii K, Susan M A B and Watanabe M 2005 *J. Phys. Chem.* B **109** 6103
[37] Shigeto S and Hamaguchi H-O 2006 *Chem. Phys. Lett.* **427** 329
[38] Iwata K, Okajima H, Saha S and Hamaguchi H-O 2007 *Acc. Chem. Res.* **40** 1174
[39] Mizuhata M, Maekawa M and Deki S 2007 *ECS Trans.* **3** 89
[40] Atkin R and Warr G G 2008 *J. Phys. Chem.* B **112** 4164
[41] Dzyuba S V and Bartsch R A 2002 *ChemPhysChem* **3** 161
[42] Nishikawa K and Iijima T 1984 *Bull. Chem. Soc. Japan* **57** 1750
[43] Caminiti R, Carbone M, Mancini G and Sadun C 1997 *J. Mater. Chem.* **7** 1331
[44] Caminiti R, Carbone M, Panero S and Sadun C 1999 *J. Phys. Chem.* B **103** 10348
[45] Nishikawa K and Kitagawa N 1980 *Bull. Chem. Soc. Japan* **53** 2804
[46] Narayanan T, Diat O and Bosecke P 2001 *Nucl. Instrum. Methods* A **467** 1005
[47] Giraud G, Karolin J and Wynne K 2003 *Biophys. J.* **85** 1903
[48] Ryu S and Stratt R M 2004 *J. Phys. Chem.* B **108** 6782
[49] Hu Z, Huang X, Annapureddy H V R and Margulis C J 2008 *J. Phys. Chem.* B **112** 7837
[50] Tao G and Stratt R M 2006 *J. Phys. Chem.* B **110** 976
[51] Elola M D, Ladanyi B M, Scodinu A, Loughnane B J and Fourkas J T 2005 *J. Phys. Chem.* B **109** 24085
[52] Elola M D and Ladanyi B M 2006 *J. Phys. Chem.* B **110** 15525
[53] Turton D A and Wynne K 2008 *J. Chem. Phys.* **128** 154516
[54] Cang H, Novikov V N and Fayer M D 2003 *J. Chem. Phys.* **118** 2800
[55] Cang H, Novikov V N and Fayer M D 2003 *Phys. Rev. Lett.* **90** 197401
[56] Johari G P and Goldstein M 1970 *J. Chem. Phys.* **53** 2372
[57] Cang H, Jie L and Fayer M D 2003 *J. Chem. Phys.* **119** 13017
[58] Li J, Wang I, Fruchey K and Fayer M D 2006 *J. Phys. Chem.* B **110** 10384